



1 Evolution of source attributed organic aerosols and gases in a 2 megacity of central China

3 Siyuan Li ¹, Dantong Liu ^{1,*}, Shaofei Kong ^{2,*}, Yangzhou Wu ¹, Kang Hu ¹, Huang Zheng ², Yi Cheng
4 ², Shurui Zheng ², Xiaotong Jiang ¹, Shuo Ding ¹, Dawei Hu ³, Quan Liu ⁴, Ping Tian ⁵, Delong Zhao ⁵,
5 Jiujiang Sheng ⁵

6 ¹ Department of Atmospheric Sciences, School of Earth Sciences, Zhejiang University, Hangzhou 310027, China

7 ² Department of Atmospheric Sciences, School of Environmental Studies, China University of Geosciences, Wuhan, 430074,
8 China

9 ³ Centre for Atmospheric Sciences, School of Earth and Environmental Sciences, University of Manchester, Manchester M13
10 9PL, UK

11 ⁴ State Key Laboratory of Severe Weather & Key Laboratory of Atmospheric Chemistry of CMA, Chinese Academy of
12 Meteorological Sciences, Beijing 100081, China

13 ⁵ Beijing Key Laboratory of Cloud, Precipitation and Atmospheric Water Resources, Beijing Meteorological Service, Beijing
14 100089, China; Field Experiment Base of Cloud and Precipitation Research in North China, China Meteorological
15 Administration, Beijing 100089, China.

16

17 *Correspondence to:* Dantong Liu (dantongliu@zju.edu.cn); Shaofei Kong (kongshaofei@cug.edu.cn)

18 **Abstract.** The secondary production of the oxygenated organic aerosol (OOA) impacts air quality, climate and human
19 health. The importance of various sources in contributing to the OOA loading and associated different aging mechanisms
20 remains to be elucidated. Here we present concurrent observation and factorization analysis on the mass spectra of organic
21 aerosol (OA) by a high-resolution aerosol mass spectrometer and volatile organic compounds (VOCs) by a proton-transfer-
22 reaction mass spectrometer in Wuhan, a megacity in central China during autumn. The full mass spectra of organics
23 with two principle anthropogenic sources were identified as the traffic and cooking sources, for their primary emission
24 profiles in aerosol and gas phases, the evolutions, and their respective roles in producing OOA and secondary VOCs.
25 Primary emissions in gas and aerosol phases both contributed to the production of OOA. The photooxidation of traffic
26 sources from morning rush-hour caused 2.5-folds increase of OOA mass in a higher oxidation state (O/C=0.72), coproducing
27 gas-phase carboxylic acids; while at night, cooking aerosols and VOCs (particularly acrolein and hexanal) importantly
28 caused the nocturnal formation of oxygenated intermediate VOCs, increasing OOA mass by a factor of 1.7 (O/C=0.42). The
29 daytime and nighttime formation of secondary aerosols as contributed by different sources, was found to be modulated by
30 solar radiation and air moisture respectively. The environmental policy should therefore consider the primary emissions and
31 their respective ageing mechanisms influenced by meteorological conditions.



32 1 Introduction

33 The transformation between gas and aerosol phase of organic species produces secondary organic aerosols (SOA)
34 (Claeys et al., 2004; Kroll and Seinfeld, 2008; Hallquist et al., 2009; Slowik et al., 2010), which forms important global
35 budget of aerosol loadings (Heald et al., 2005; Zhang et al., 2007), exerting climate (Poschl, 2005; Seinfeld et al., 2016) and
36 environmental impacts (Von Schneidmesser et al., 2011; Huang et al., 2014). Given the large complexities of organic
37 species, the yields (Goldstein and Galbally, 2007; Ortiz-Montalvo et al., 2014) and production rates (Sareen et al., 2013;
38 Jokinen et al., 2015) of SOA from gas precursors are influenced by the diversities of source profiles (emission mass
39 percentages among species) (Lin et al., 2012; Shrivastava et al., 2015) and environmental factors (such as radiation, air
40 moisture and ambient temperature) (Li et al., 2021b; Wang et al., 2021). This raises challenges for source-oriented
41 environmental policy making, before explicit understanding on the formation mechanism of SOA from different sources.

42 The application of detailed mass spectra of organic aerosols allows online source attribution of organic aerosol (OA)
43 (Canagaratna et al., 2007; Ng et al., 2011), based on the factorization analysis on the mass spectra of OA which groups the
44 covaried species from certain sources (Ulbrich et al., 2009). This factorization technique allows identification of primary
45 sources and aged secondary sources at a receptor measurement site. The complex aerosol sources in urban environment have
46 been commonly recognized as traffic sources mainly from vehicles on road (Zhu et al., 2021), biomass burning from open or
47 closed combustion (Adler et al., 2011), coal combustion normally in cold season for heating (Xu et al., 2019) and more
48 localized cooking sources (Allan et al., 2010; Zhang et al., 2020b). The secondary sources are oxygenated OA which may be
49 from oxidizing volatile organic compounds (VOCs) following condensation (Donahue et al., 2006), or heterogenous
50 oxidation occurring on particle phase (Claeys et al., 2004; Kroll and Seinfeld, 2008). Among these sources, SOA has been
51 found to be the main contributor of OA mass loading (41~69%) in urban environment of East Asia (Sun et al., 2014; Hu et
52 al., 2017), especially in warm season when primary emissions were low, along with high ambient temperature and more
53 intensive chemical reactions (Hu et al., 2016). The formation of SOA from VOCs may experience a few reaction generations
54 (Knote et al., 2014) and could interact with other sources of species during the process (Shrivastava et al., 2017), hereby
55 complicating the goal of identifying the key precursors in contributing to the consequent SOA. In addition, some primary
56 gases already have somehow low volatility and may not require a long reaction chain to become condensable, such as some
57 primarily emitted intermediate volatility organic compounds (IVOCs) may substantially contribute to the SOA (Robinson et
58 al., 2007; Huang et al., 2021). An understanding of source profiles of primary emissions in both gas and aerosol phases is
59 therefore important to rule out the source-dependant production of SOA. The above necessitates the concurrent investigation
60 on the compositions of gases and aerosols at a receptor site, along with their evolution and interaction, in order to elucidate
61 the role of each source in contributing to SOA.

62 In this study, we performed online continuous measurements on the detailed mass spectra of organics concurrently on
63 aerosol and gas phases, in a typical anthropogenically polluted region in central China, where such data had been rarely



64 reported. Factorization analysis is performed on the mass spectra of organics in both aerosol and gas phases, to investigate
65 the source-oriented gas-aerosol evolution and SOA formation in this region.

66 **2 Materials and methods**

67 **2.1 Sampling site**

68 The field experiment was performed in the campus of the China University of Geosciences (Wuhan) (114.40° E, 30.52°
69 N) during Oct.- Nov. 2019 (Hu et al., 2021). The site represents a typical residential/traffic mixed region (Fig. S1). Due to
70 the preparation and hosting of the 7th CISM Military World Games during the experimental period, the government
71 implemented strict emission reduction measures, particularly for industrial sources. The local pollution sources were hereby
72 dominated by traffic and cooking sources, besides those transported from surrounding regions during some heavy pollution
73 events (Zheng et al., 2019; Zheng et al., 2020). The HYSPLIT model (Draxler and Hess, 1997) with a 3-hourly 1° × 1° wind
74 field from the GDAS reanalysis products was used to obtain the 36-h backward trajectories initialized from the location of
75 the experiment site. Cluster analysis was performed to categorize the trajectories into three groups by minimizing the
76 differences in each group and maximizing the differences among groups (Moody and Galloway, 1988).

77 **2.2 Instrumentation**

78 **2.2.1 Measurements of mass spectra of aerosols and gases**

79 The mass concentration and chemical composition of NR-PM₁ were measured by a HR-ToF-AMS (Aerodyne Research
80 Inc., USA), including organics, nitrate (NO₃⁻), sulphate (SO₄²⁻), chloride (Cl⁻), and ammonium (NH₄⁺). The detailed can be
81 found elsewhere (Decarlo et al., 2006). Briefly, the aerosols are dried using a diffusion dryer before entering the AMS and
82 through a critical orifice into a narrow beam via an aerodynamic lens. The aerosol size is determined using the flight time of
83 particles to the thermal vaporization and ionization chamber. Then the aerosols are successively vaporized by a heated
84 surface (~600 °C), ionized by electron ionization (EI, 70 eV), and detected by a mass spectrometer detector. During this field
85 observation, the HR-ToF-AMS was operated under V mode with high sensitivity. The composition-dependent collection
86 efficiencies (Middlebrook et al., 2012) were applied, and the ionization efficiency was calibrated using 300 nm pure
87 ammonium nitrate (Jayne et al., 2000). Elemental analysis (EA) was also executed using the “Improved Ambient” method
88 (Canagaratna et al., 2015) to obtain the hydrogen-to-carbon ratio (H/C), oxygen-to-carbon ratio (O/C), and nitrogen-to-
89 carbon ratio (N/C).

90 The Proton-Transfer-Reactor Time-of-Flight Mass Spectrometer (PTR-ToF-MS 8000, Ionicon Analytik GmbH
91 Innsbruck, Austria) was deployed to quantify VOCs in this research. The operating and calibration of the PTR followed the
92 routine described previously (Cappellin et al., 2012; Bruns et al., 2016). Briefly, the PTR was operated with hydronium ions
93 (H₃O⁺) as the reagent and with a drift tube pressure of 2.2 mbar, voltage of 600 V and temperature of 60 °C. The ratio of the
94 electric field (*E*) and the density of the buffer gas (*N*) in the drift tube, which dictates the ion drift velocity in the drift tube, is



95 135 Td. MS transmission function was performed using a mixture of VOCs (formaldehyde, methanol, acetonitrile,
96 acetaldehyde, acetone, isoprene, methyl ethyl ketone, benzene, toluene, styrene, benzaldehyde, ethylbenzene, 1,3,5-
97 trimethylbenzene). Mass calibration was done using H_3O^+ (m/z 21.0226), $\text{CH}_3\text{COCH}_4^+$ (m/z 59.0490) and monoterpenes (m/z
98 137.1290). The shift in m/z is minor which ensures that the mass calibration was sufficient for all compounds. The
99 background measurements were performed using a dry zero air cylinder. The measurement error is described in Text S2. A
100 separate reaction rate constant is applied to convert the ion signal into concentration (Bruns et al., 2016), or the default
101 reaction rate constant $2 \times 10^{-9} \text{ cm}^3 \text{ s}^{-1}$ can be applied to all other ions (Wang et al., 2020b). The vapor saturation concentration
102 (equilibrium vapor pressures) (C^*) of each VOCs compound at 25°C is estimated using the parameterization based on
103 elemental ratio and molecular weight (Fig. S2) (Li et al., 2016). A $\log C^*$ (in $\mu\text{g m}^{-3}$) lower than 6.5 is deemed to be
104 intermediate VOC (IVOC). According to Fig. S2, VOC species (with $m/z > 120$) are mainly identified to be IVOCs in this
105 study, thus the fraction of these larger molecular weight (MW) VOCs ($m/z > 120$) is used to evaluate the potential influence
106 of IVOCs.

107 2.2.2 PMF analysis on the mass spectra of OA and VOCs

108 Positive matrix factorization (PMF) (Paatero and Tapper, 1994) was performed on the high-resolution organic mass
109 spectral matrix of OA (Ulbrich et al., 2009; Decarlo et al., 2010). In this work, $m/z > 120$ and isotopic ions were excluded in
110 PMF analysis due to the limited mass resolution and low contributions to OA loading ($\sim 5\%$). After a careful evaluation of
111 the mass spectral profiles and correlations with time series of tracers, diurnal variations, four OA factors from total OA were
112 identified with $f_{\text{peak}} = 0$, including hydrocarbon-related OA (HOA), cooking OA (COA), low-oxidized oxygenated OA
113 (LO-OOA, OOA1), and more-oxidized oxygenated OA (MO-OOA, OOA2). The detail of PMF diagnostic was summarized
114 in Text S1 and Fig. S3.

115 The EPA PMF 5.0 model (Paatero and Tapper, 1994) was used for the source apportionment of VOC species. The 109
116 VOCs were used for the PMF analysis. The uncertainties from each sample were determined according to the method
117 detection limit (MDL) and the error fraction (%). The detail of PMF diagnostic was summarized in Text S2 and Fig. S4. Five
118 factors were ultimately selected, and the Q/Q_{exp} ratio was 0.96 on average (Fig. S4). The rotation ambiguity was explored by
119 varying the f_{peak} values from -3 to +3, and the results with $f_{\text{peak}} = 0$ were selected for the lowest dQ (robust), indicating the
120 stability of the PMF solution (Zhou et al., 2019). Most of the residuals are distributed normally, ranging from -3 and +3,
121 suggesting the model fit the input data well.

122 2.2.3 Other measurements

123 The concentration of BC particles was measured by a single particle soot photometer (SP2, DMT Inc.). The operation
124 and data analysis procedures of the SP2 have been described elsewhere (Schwarz et al., 2008; Liu et al., 2010). The SP2
125 incandescence signal was calibrated for refractory BC (rBC) mass using the Aquadag black carbon particle standards
126 (Acheson Inc., USA) and corrected for ambient rBC with a factor of 0.75 (Laborde et al., 2012).



127 The size distribution and number concentration of aerosols with a mobility diameter from 12 to 552 nm were also
128 measured by a scanning mobility particle sizer (SMPS, Model 3081, impactor 50% cut off at 0.677 μm ; CPC model 3775 at
129 a flow rate 0.3 L/min). PM_{10} mass concentration calculated based on the volume concentration measured by the SMPS agreed
130 well with that from the sum of compositions by the HR-ToF-AMS and SP2 ($r=0.71$).

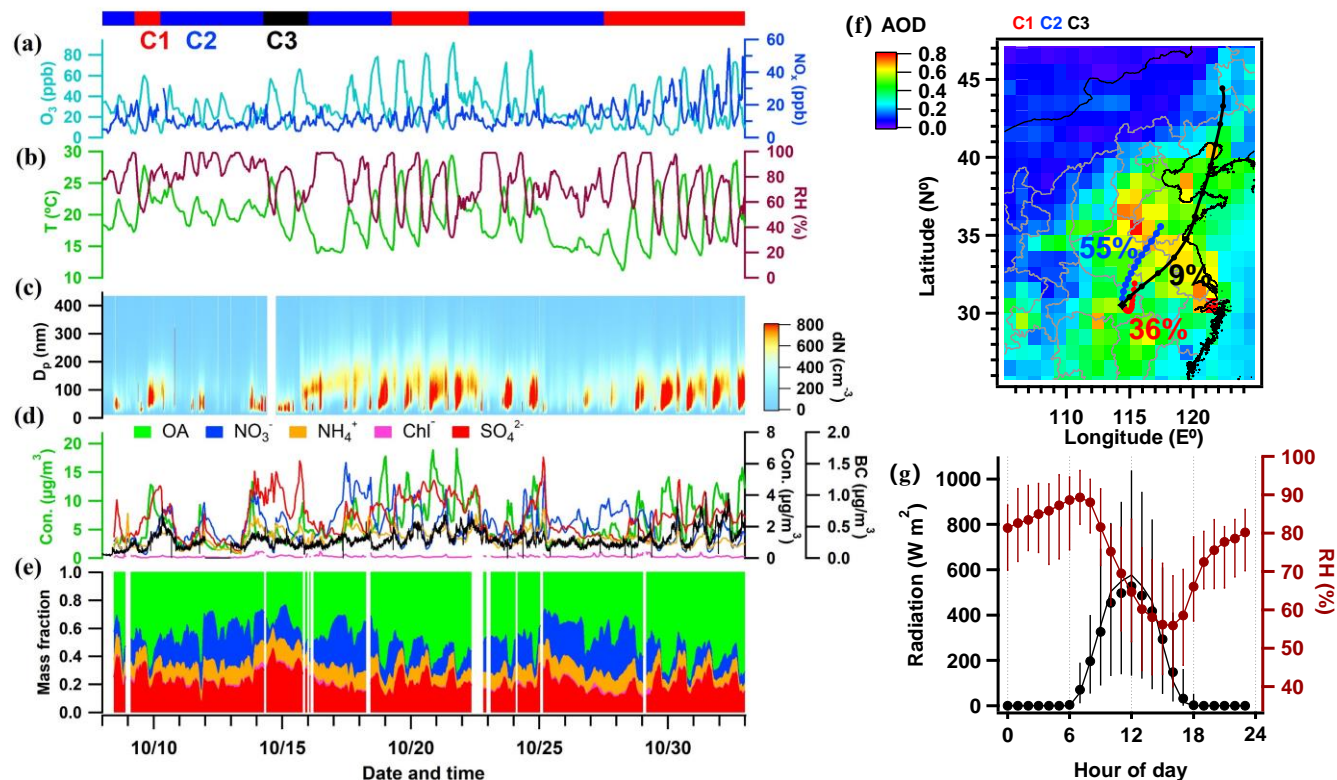
131 The gas-phase species including NO_x , O_3 , and CO were measured in real time by a series of Wuhan Tianhong analyzers
132 (TH-2001H, TH-2003H, TH-2004H, respectively). These instruments were calibrated periodically with the corresponding
133 standard gas to ensure the accuracy of the observation data. In addition, the meteorological parameters including temperature
134 (T), relative humidity (RH), and wind speed and direction were recorded by an automatic weather station.

135 3 Results and discussion

136 3.1 Chemical compositions of PM_{10}

137 The time series of mass concentrations of BC, nonrefractory- PM_{10} (NR- PM_{10}) species (i.e., OA, SO_4^{2-} , NO_3^- , NH_4^+ , and
138 Cl⁻) and their relative contributions are summarized in Fig. 1. During this field observation, the mass concentrations of NR-
139 PM_{10} were in the range of 2.5 - 44.8 $\mu\text{g m}^{-3}$, with an average of $12.7 \pm 5.7 \mu\text{g m}^{-3}$, which is close to those observed in the
140 North China Plain in autumn 2019 ($15.1 \mu\text{g m}^{-3}$) (Li et al., 2021a), and was much lower than that ($41.3 \pm 42.7 \mu\text{g m}^{-3}$)
141 observed in Beijing in autumn 2012 (Hu et al., 2017). The mean mass concentration of BC was $0.29 \pm 0.17 \mu\text{g m}^{-3}$ with the
142 range of 0.1 - 1.0 $\mu\text{g m}^{-3}$. Among all species in NR- PM_{10} , OA contributed the major (49.2 %), indicating the dominant role of
143 OA in autumn time of PM_{10} pollution in this region. Inorganic aerosol accounted for 50.8 % of NR- PM_{10} in which sulfate was
144 the largest contributor (21.5 %), followed by nitrate (18.5 %), ammonium (10.7 %), and chloride (0.1 %), which has similar
145 relative contributions to those observed in field (Chen et al., 2021). The number concentration of all particles peaked at $95 \pm$
146 38 nm^{-3} in with regular growth during every field day. Fig. 1 also presents the time series variation in meteorological
147 parameters. During the field observation period, the average temperature and relative humidity (RH) were $19.3 \pm 3.6 \text{ }^\circ\text{C}$
148 ($11.2\text{--}29.4 \text{ }^\circ\text{C}$) and $75.0 \% \pm 17.5 \%$ ($25.0\% \text{--}99.0\%$), respectively. The O_3 concentration with an average of 30.7 ± 13.0
149 ppb, was highest 54.5 ppb at 15:00, likely due to the high temperatures and enhanced photochemical processing.

150 Fig. 1f shows the spatial distribution of aerosol optical depth (AOD) and 36 h backward trajectories during the
151 campaign. Cluster-1 (C1) shows the circulated air mass with shortest transport distance for the past 36 h (36% fraction); C2
152 is the northerly transported air mass (55% fraction), over regions with higher AOD; C3 is the most rapid transport through
153 the northeast China and some coastal areas. Fig. 1g shows the diurnal variations of solar radiation and RH, peaking in the
154 day and night respectively.



155

156 **Figure 1:** Time series of (a) mass concentrations of O₃ and NO_x; (b) ambient temperature (T) and relative humidity (RH); (c)
157 number size distribution measured by the SMPS; (d) mass concentrations of key aerosol species; (e) mass fractions of chemical
158 species in non-refractory PM₁; (f) spatial distribution of mean aerosol optical depth (AOD) during the experiment and the
159 clustered 36 h backward trajectories; (g) diurnal profiles of direct solar radiation and RH.

160 3.2 Source attributed organic aerosol

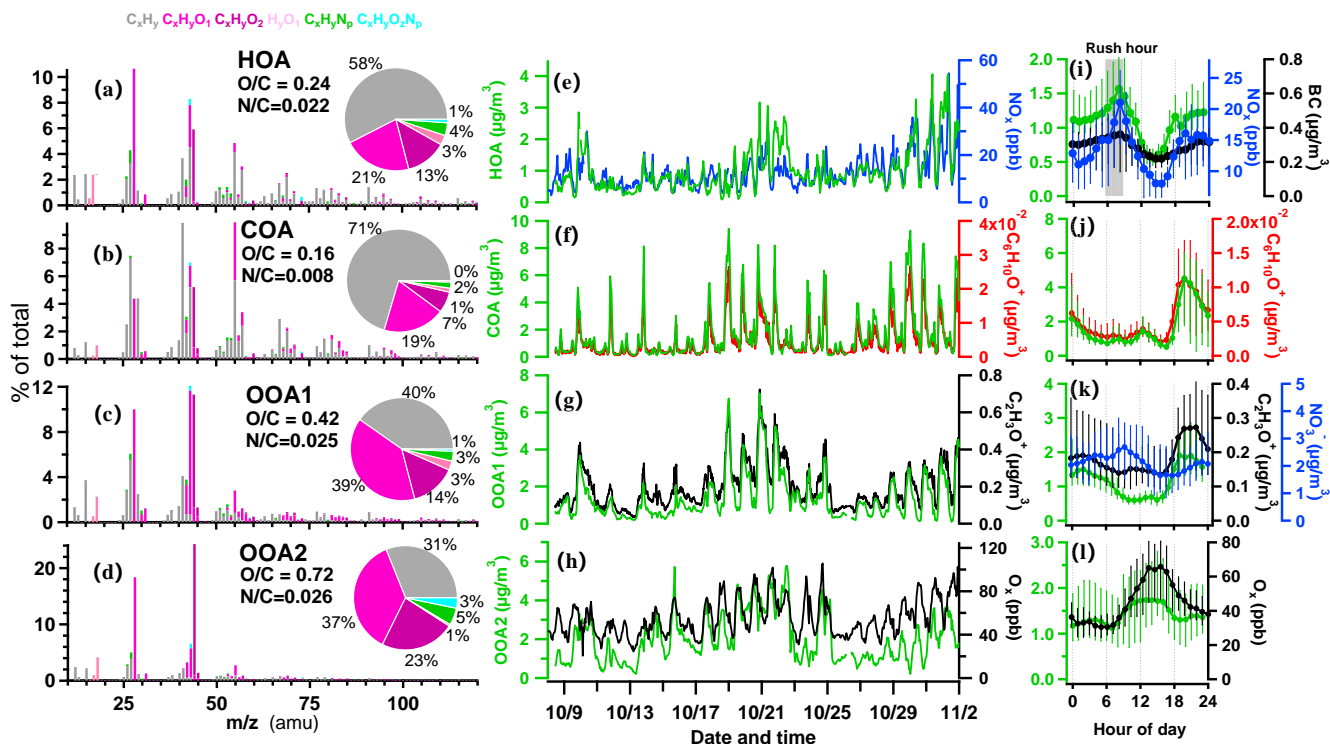
161 The resolved OA factors by the PMF analysis on the AMS measurements are shown in Fig. 2. The first factor is
162 characterized by prominent hydrocarbon ion series of C_nH_{2n-1}⁺ and C_nH_{2n+1}⁺ (Fig. 2a), with a low O/C ratio (0.24), which is
163 generally considered to be related to the emissions of fossil fuel combustion and vehicle emissions (Huang et al., 2010;
164 Morgan et al., 2010; N. L. et al., 2011). The time series of the factor correlated well with NO_x (r = 0.71) and BC (r = 0.83)
165 (Fig. 2e and Table S1). The diurnal pattern of this factor showed peaks in the morning and afternoon rush-hour (Fig. 2i),
166 with a major increase from 5:30, reaching a peak value of 1.5 μg m⁻³ at 8:30. The concentration gradually decreased around
167 noontime due to boundary layer dilution until 15:00 and reached a minimum of 0.6 μg m⁻³. This spectrum also contained
168 fragment marker for possible coal combustion OA (CCOA), i.e. C₉H₇⁺ (m/z 115, r = 0.73) (Hu et al., 2013). This factor was
169 not distinctly resolved in this dataset maybe due to the urban nature of the site, where the traffic source may have
170 overwhelmed, due to the less significant coal combustion pollutants during the sampling period.



171 The second factor was characterized by m/z 55 ($C_4H_7^+$, $C_3H_3O^+$) and 57 ($C_4H_9^+$, $C_3H_5O^+$), accounting for 10% and 3.5%
172 of the total spectrum, respectively (Fig. 2b), with the lowest O/C ratio among factors (0.16). This factor has a
173 $C_3H_3O^+/C_3H_5O^+$ of 3 and $C_4H_7^+/C_4H_9^+$ of 2 (1 is usually for HOA), indicating it as cooking source rather than HOA (Mohr et
174 al., 2012). The correlation coefficient of the COA factor and marker ion $C_6H_{10}O^+$ was 0.91, which is also similar to a
175 previous study (Sun et al., 2011). The diurnal pattern of this factor showed a major peaking during 18:00 - 20:00, reaching
176 up to $4.0 \mu\text{g m}^{-3}$ on average, in addition to a smaller peak at lunch time, which corroborated the diurnal cooking activities.
177 Previous studies reported COA accounted for 6.5 - 30 % of the total OA in urban (Rogge et al., 1991; Lanz et al., 2008;
178 Allan et al., 2009; Xu et al., 2014). Here the concentrations and proportions of COA in OA were in the range of 0.5 - $4.5 \mu\text{g}$
179 m^{-3} and accounted for 23 % of OA on average. The cooking emission in the studying region was likely from charcoal-
180 grilling activities, which are popular in the surrounding areas.

181 Besides the two primary OA, additional two oxygenated OA (OOA) factors are identified. According to the oxidation
182 state, OOA was further separated into lower (OOA1) and more oxidized (OOA2) factors. OOA1 factor contained abundant
183 oxygen-containing fragments, accounting for more than 50% of the total mass spectrum, with an O/C of 0.42. In particular,
184 oxygenated fragment containing one oxygen accounted for 39%. The $C_2H_3O^+$ ion (m/z 43) is an important component of less
185 oxidized SOA (Wang et al., 2020a), which was highly correlated with OOA1 ($r = 0.94$). OOA1 showed lower concentration
186 during daytime and higher concentration during nighttime (Fig. 2k). Such diurnal variation was similar to that of RH, but
187 opposite to that of solar radiation, which was similar to the previous report (Sun et al., 2014). OOA1 may thus be associated
188 with aqueous reactions when high RH. The co-occurrence of nighttime peak of OOA1 and COA suggested the primary
189 source of cooking emission may have considerably contributed to the production of OOA1.

190 The factor OOA2 had the highest O/C of 0.72 and contained 61% oxygen-containing fragments (Fig. 2d), which is very
191 similar to the spectra of OOA factor resolved in other cities (Aiken et al., 2009; Hayes et al., 2013). This factor was
192 correlated strongly with the fragment of CO_2^+ ($r=0.79$). Compared to OOA1, this factor showed obvious diurnal variations
193 with a major enhancement of around noontime (10:00-15:00), up to $2.9 \mu\text{g m}^{-3}$, indicating photochemical production of SOA
194 during daytime. The variation of OOA2 also correlated with odd oxygen ($O_x=O_3+NO_2$). These features agree well with the
195 previous observation of characteristic of more oxidized OA (Hu et al., 2016).



196
 197 **Figure 2: Results of source-attributed organic aerosols by the PMF analysis on the OA mass spectra measured by the HR-TOF-**
 198 **AMS. Mass spectra of PMF factors for (a) hydrocarbon-like OA (HOA); (b) cooking OA (COA); (c) oxygenated OA1 (OOA1); (d)**
 199 **oxygenated OA2 (OOA2). The pies show the relative contributions of the six ion categories to each factor. (e-h) Temporal**
 200 **variations of four OA factors (HOA, COA, OOA1 and OOA2) with each correlated species as NO_x , $\text{C}_6\text{H}_{10}\text{O}^+$, $\text{C}_2\text{H}_3\text{O}^+$ and O_x . (i-l)**
 201 **Diurnal profiles of NO_x , BC, $\text{C}_6\text{H}_{10}\text{O}^+$, $\text{C}_2\text{H}_3\text{O}^+$, NO_3^- and O_x . The lines and whiskers denote the median, the 25th and 75th**
 202 **percentiles at each hour, respectively.**

203 3.3 Source attributed VOCs

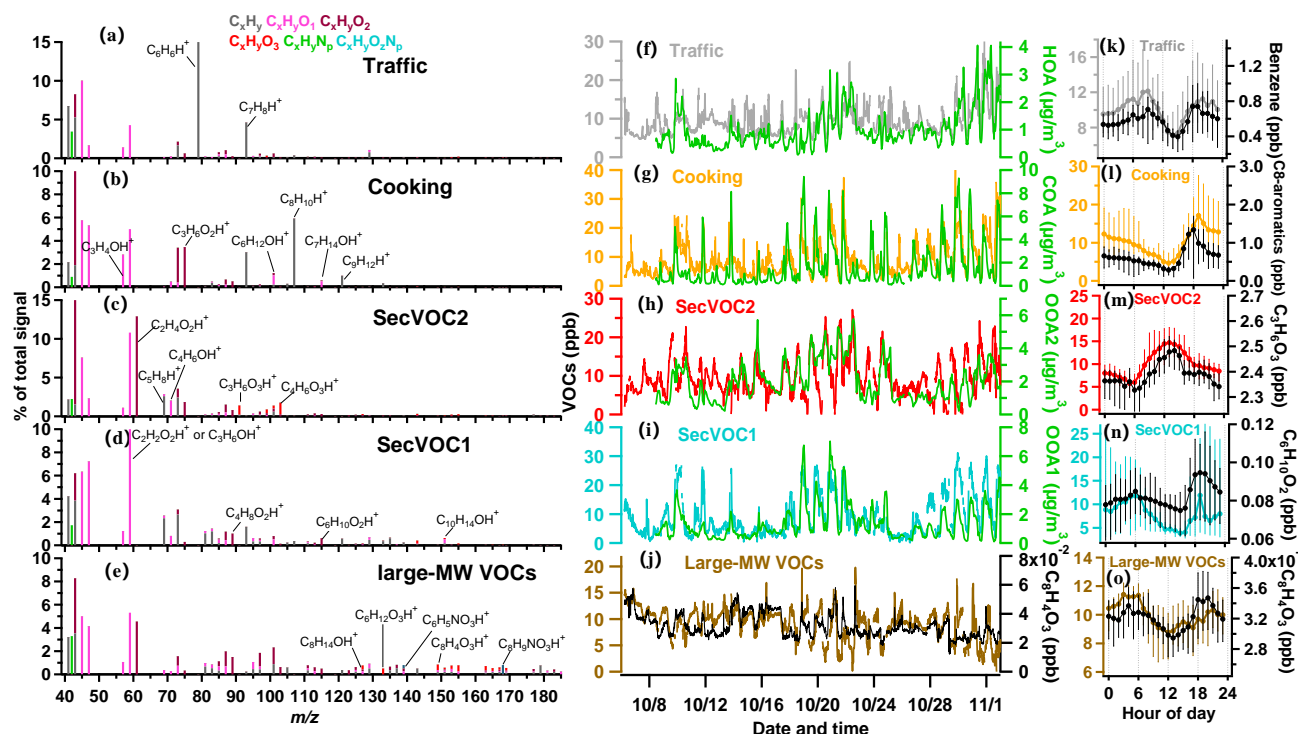
204 Fig. 3 and Fig. S5 summarize the source attributed of VOCs and key indicators. The first factor is dominated by
 205 aromatic compounds, such as C_6H_6 (m/z 79.054) and C_7H_8 (m/z 93.070) in Fig. 3a, which are well established markers for
 206 vehicle emissions (Gkatzelis et al., 2021), with good correlations of this factor ($r = 0.97$ and 0.63 , respectively Fig. S6). This
 207 factor showed peaks in the morning and afternoon rush-hour (Fig. 3k) and was well correlated with HOA and NO_x ($r = 0.63$
 208 and 0.53 Table S1), with a major increase during the early morning, reaching a peak value of 12.1 ± 1.3 ppb at 08:30, further
 209 corroborating the traffic source of this factor. The concentration decreased around noontime until 15:00 because of the
 210 dilution by well-developed boundary layer and its consumption through photochemical reaction due to intense solar
 211 radiation. The diurnal pattern was also high at night, although the peak was lower than early morning, the average
 212 concentration was higher by a factor of 2 than daytime. This suggests that traffic VOCs prefer to participate in
 213 photochemical reaction, and other primary emissions may be precursors during nocturnal chemistry.



214 The second factor contained abundant aldehydes such as C_3H_4O (acrolein), $C_3H_6O_2$ (hydroxyacetone), $C_6H_{12}O$
215 (hexanal), and $C_7H_{14}O$ (heptanal) at m/z 57.069, 75.044, 101.096, and 115.112, respectively, as well as C_8H_{10} (C8-aromatics)
216 and C_9H_{12} (C9-aromatics) at m/z 107.086 and 121.101 in VOC mass spectra (Fig. 3b), which are footprint VOCs identified
217 from primary cooking emission during the charbroiling and frying (Klein et al., 2016). This factor had similar time series
218 (Fig. 3g) with COA and had high correlation ($r=0.67$, Table S1). The concentration of this factor decreased during the
219 daytime, and yet surged after 18:00 with a peak value at 19:00 (17.2 ± 3.0 ppb). As shown in Fig. 3l, the diurnal pattern
220 decreased strongly after emission throughout the night, suggesting that cooking VOCs may be major precursors and were
221 consumed during night.

222 Besides the two primary VOCs, three secondary oxygenated VOCs (SecVOCs) factors are identified. These three
223 factors are not well correlated with any primary factors attributed by the OA, are thus considered to be mainly contributed by
224 secondary production. Among these three factors, SecVOC2 contained isoprene (C_5H_8 , at m/z 69.070), and also some first
225 generation oxidation product, methyl vinyl ketone and methacrolein (MVK+MACR, m/z 71.049), which were produced by
226 enhanced biogenic emission of vegetations under solar radiation (Jordan et al., 2009; Cheng et al., 2018; Zhang et al., 2020a;
227 Gu et al., 2021). This factor was thus also contributed by this primary source. SecVOC2 contributed a large fraction of
228 $C_2H_4O_2$, $C_3H_6O_3$ and $C_4H_6O_3$ (Fig. 3c), which were gas-phase carboxylic acids, the oxidation products from photochemical
229 processes (Hartikainen et al., 2018; Li et al., 2021b). SecVOC2 had one clear peak at 13:00 (14.7 ± 2.8 ppb Fig. 3m). The
230 time series of SecVOC2 correlated well with OOA2 ($r = 0.67$), following the variation of solar radiation. It had a rapid
231 enhancement starting from 07:00 to 12:00 and declined continuously after 13:00. This indicated that many of these species
232 can be formed rapidly during daytime and may have a short lifetime owing to the partitioning to the condensed phase and
233 forming SOA.

234 SecVOC1 factor featured with some less-oxygenated VOCs e.g., $C_2H_2O_2$, $C_6H_{10}O_2$ and $C_{10}H_{14}O$ (Fig. 3d). This factor
235 had a peak at 19:00 which was consistent with the primary cooking VOCs factor, but also increased throughout the night,
236 peaking at midnight. This factor had a similar temporal trend with OOA1 ($r = 0.76$, Fig. 3i), which was less oxygenated than
237 photochemistry dominated OOA2. Combining the features above, SecVOC1 tended to be contributed by some immediately
238 reacted species from emissions in the late afternoon and early night. A particular factor (Fig. 3e) is significantly composed of
239 large molecular weight (large-MW) oxidized VOCs, i.e. the average on relative contribution of ionic compounds with
240 $m/z > 120$ was above 50% in this factor (Fig. S5e), which was much higher than that in SecVOC2 (Fig. S5c). Fig. 3e shows
241 its signature compounds of $C_8H_{14}O$, $C_6H_{12}O_3$ and $C_8H_4O_3$, and some are nitrogen-containing VOCs, such as $C_6H_5NO_3$ and
242 $C_8H_9NO_3$. These VOCs with $m/z > 120$ tend to be intermediate-volatility organic compounds (IVOCs) as the estimated vapor
243 saturation concentration is less than $6.5 \mu g m^{-3}$ (Fig. S2). This factor is hereby termed as large-MW VOCs to indicate the
244 fraction of IVOCs, which only require few oxidation steps to become semi-volatile (Robinson et al., 2007). Fig. 3o shows an
245 increase of this factor at mid-night, later than the peak of SecVOC1, which may imply the ageing process in producing these
246 VOCs.



247
 248 **Figure 3.** Source attributed VOCs by the PMF analysis measured by the PTR-TOF-MS. (a-e) Mass spectra of the five factors
 249 (traffic VOCs, cooking VOCs, secondary VOCs (SecVOC2, SecVOC1) and large molecular weight (MW) VOCs (large-MW
 250 VOCs), with major fingerprint peaks labelled in the mass spectra. (f-j) Temporal variations of the five VOCs factors and their
 251 respective correlated OA species. (k-o) Diurnal profiles of the VOC factors and their respective signature species. The lines and
 252 whiskers denote the median, the 25th and 75th percentiles at each hour, respectively.

253 3.4 Oxidation process of organics in the day and night

254 After source attribution of organics in aerosol and gas phase, we are able to identify the emission structure of primary
 255 sources and the consequent evolution. Given the identified primary traffic and cooking sources were emitted in the day and
 256 late afternoon respectively, this provides the potential opportunity to study the evolution of different primary sources in the
 257 potentially contrasting ageing mechanisms in the day and night.

258 Fig. 4a-d shows the temporal evolution of the key factors in a week to reflect the day and night ageing. The O/C ratio in
 259 the day is higher than that at night by 0.2 (Fig. 4a), corresponding with the increase of highly oxygenated fragments of AMS
 260 f_{44} (CO_2^+) in the day (Fig. 4b), but increase of moderately oxygenated fragment f_{43} ($C_2H_3O^+$) in the night. The diurnal
 261 variation of atomic ratio O/C of OA (Fig. 4e) showed a slight decrease at morning rush-hour and sharp drop at 18:00 (by 0.2)
 262 due to the significant contribution of the traffic and cooking sources respectively, corresponding with the two steps of
 263 increase at each time. This variation of O/C clearly showed the daytime and nighttime ageing processes of OA for different
 264 primary sources. Notably, the O/C showed peak value of 0.54 at 15:00, implying the importance of photooxidation in
 265 producing highly oxygenated OA.

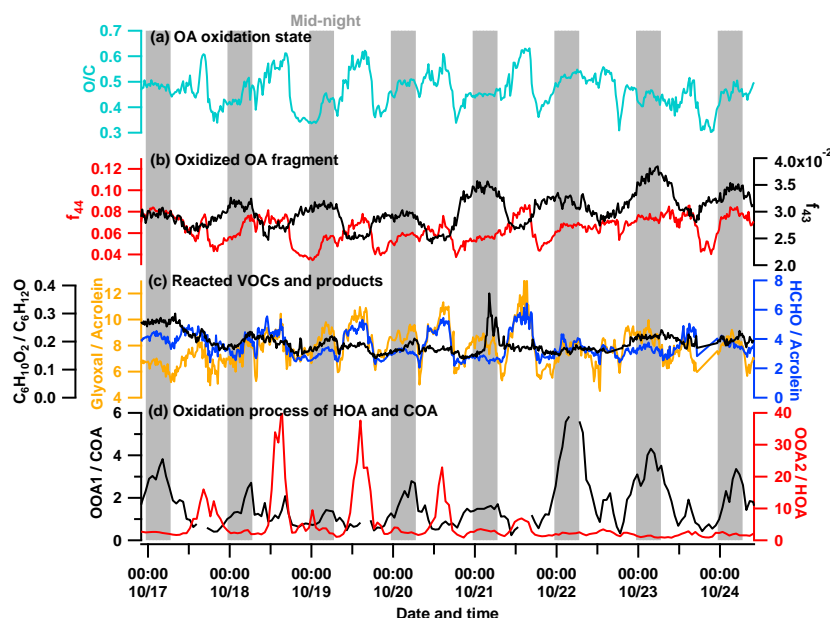


266 Considering the diurnal pattern of anthropogenic activities, the traffic emission at rush-hour is deemed to be the major
267 source in contributing to the daytime production of OOA. The ratio OOA2/HOA is thus used to indicate the daytime
268 oxidation of OOA. As Fig. 4d and 4f shown, OOA2/HOA had a clear peak during daytime, and increased after 8:00 and
269 peaked at 14:00. After 15:00, the ratio gradually decreased to minimum at 20:00 and maintained to be low throughout the
270 night. This clearly demonstrated the photooxidation in producing OOA2 from oxidizing HOA. Fig. 4c and 4g give a few
271 examples of photooxidation in gas phase: the toluene showed a production of $C_3H_6O_3$ (hydroxypropionic acid) and $C_4H_6O_3$
272 (acetic anhydride) by a factor of 2 in 3 hours (Fig. S7c); the C_3H_4O (acrolein) produced the oxidized product $C_2H_2O_2$
273 (glyoxal) by a factor of 1.3 (Fig. 4h). All of these reacted species are from traffic VOCs and the corresponding products are
274 from SecVOC2. The daytime biogenic emission, e.g. isoprene, may also contribute to the SecVOC2 formation by interacting
275 with OH in the presence of NO_x (Lin et al., 2013), producing methacrylic acid epoxide (MAE) as the intermediate involved
276 in SOA formation, where a considerable nitrogen content was also found in OOA2 factor ($N/C=0.026$). Overall, the highly
277 oxidized OOA2 ($O/C=0.72$) is considered to be mainly contributed by traffic source, via oxidation of VOCs and partitioned
278 to condensed phase, direct oxidation on HOA through heterogenous oxidation (Guo et al., 2020), or VOCs evaporated from
279 HOA and further condensed after oxidation (Zhao et al., 2015). All factors may have contributed to the daytime production
280 of OOA2.

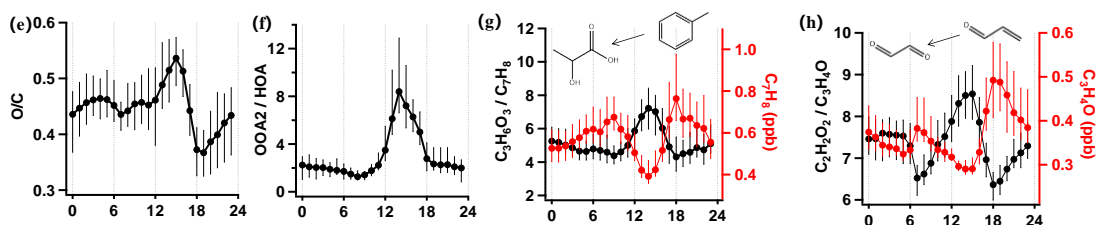
281 The nocturnal oxidation is mainly contributed by the sources emitting from late afternoon throughout the midnight.
282 Both traffic and cooking sources contributed to the emission since late afternoon, with cooking source as the predominant
283 contributor in both aerosol (Fig. 2j) and gas (Fig. 3l) phases. The ratio between the nighttime OOA1 and cooking aerosol
284 (OOA1/COA) is therefore used to indicate the nocturnal oxidation of SOA (Fig. 4d and j). There was a sudden increase of
285 OOA1/COA during the daytime because COA was consumed rapidly in the afternoon after a small amount of emission at
286 noon (Fig. 2j). The lowest OOA1/COA at 0.5 corresponded with the fresh cooking emission at 18:00, and kept increasing
287 until peaking in the early morning at 6:00 up to 3, which was an increase by a factor of 6 compared to the minima (Fig. 4j).
288 In addition to evidence for daytime reaction, Fig. 4h and Fig. S7d also gave evidence for certain reacted species during the
289 ageing at nighttime. The first-generation oxidation products from acrolein (ACR $C_3H_4OH^+$, m/z 57.033) are glyoxal
290 ($C_2H_2O_2$, m/z 59.036) and formaldehyde ($HCHOH^+$, m/z 31.018) (according to the database in Master Chemical Mechanism
291 (MCM). This night oxidation is also evidenced by the formation of some nitrated organic compounds and ketone
292 compounds, such as $C_6H_5NO_3$ (nitrophenol, NP, Fig. 4l) and $C_6H_{10}O_2$ (hexanedione, Fig. 4k) produced from phenol (C_6H_6O)
293 and hexanal ($C_6H_{12}O$), respectively. Notably, an important fraction of large molecular weight-VOCs (which are mostly
294 intermediate VOCs, Fig. S2) peaked at 3:00 - 4:00 (Fig. 3o), consistent with the variation of OOA1/COA during night. Some
295 of these nitrated and oxygenated IVOCs may have been further oxidized and partitioned to aerosol phase, contributing to the
296 OOA1. Given the larger molecular usually has a lower O/C ratio (Hatch et al., 2017) (because of a higher content of carbon),
297 this may explain the lower O/C observed for nighttime formed OOA1 ($O/C=0.42$), than OOA2 produced by daytime



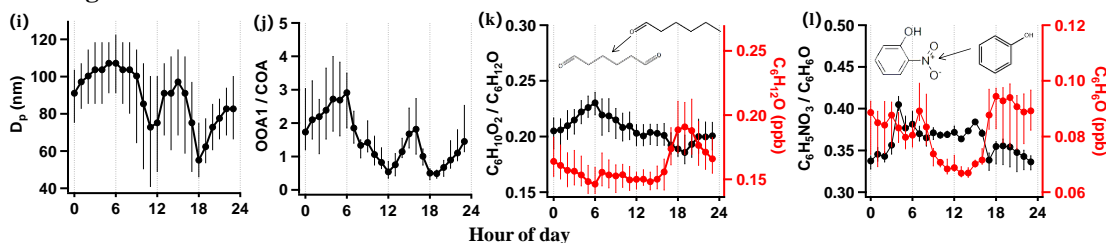
298 photooxidation ($O/C=0.72$). Notably, nighttime SOA had a high N/C (0.025), implying the NO_3^- -initiated from cooking
 299 emissions oxidation, which was different from the organic nitrate formation mechanism during the daytime.



Daytime photo-oxidation



Nighttime oxidation



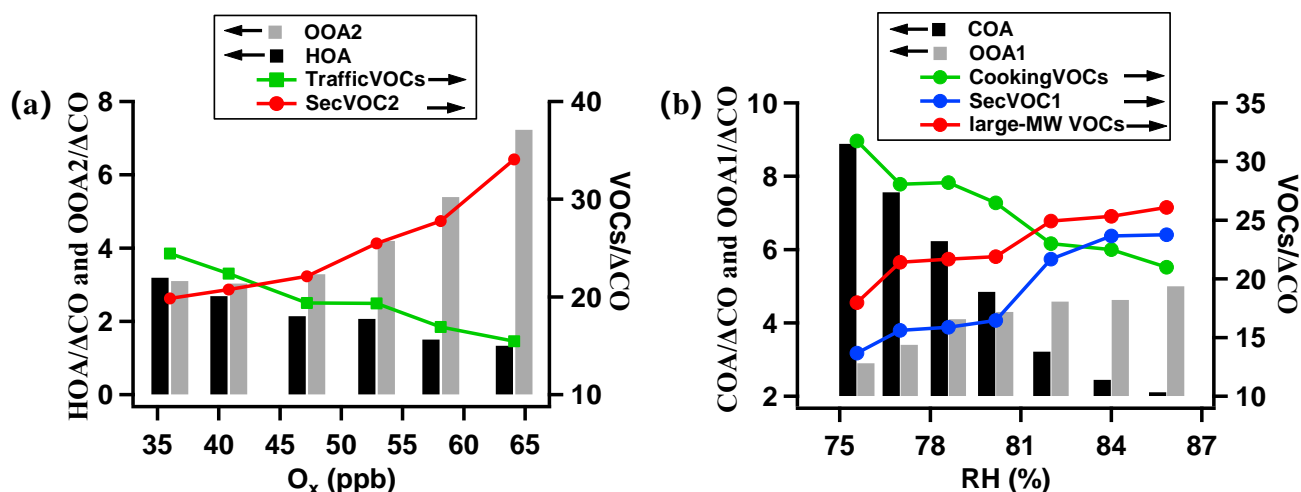
300
 301 **Figure 4.** Time series showing the aging of aerosols and gases, with grey vertical bars denoting nighttime (00:00-06:00), (a) the
 302 oxygen to carbon ratio (O/C); (b) the fragment fraction at m/z 44 (f_{44}), m/z 43 (f_{43}); (c) concentration ratio of $C_6H_{10}O_2$ to $C_6H_{12}O$
 303 (hexanedione to hexanal), glyoxal to acrolein, and formaldehyde to acrolein; (d) concentration ratio of OOA1 to COA and OOA2
 304 to HOA. Diurnal variations of key species showing the daytime photooxidation and nighttime oxidation, (e) ratio of O/C ; (f) ratio
 305 of OOA2 to HOA; (g) concentration of C_7H_8 and ratio of $C_3H_6O_3$ to C_7H_8 (hydroxypropionic acid to toluene); (h) concentration of
 306 C_2H_4O and ratio of $C_2H_2O_2$ to C_3H_4O (glyoxal to acrolein); (i) particle diameter (D_p); (j) ratio of OOA1 to COA; (k) concentration
 307 of $C_6H_{10}O_2$ and ratio of $C_6H_{10}O_2$ to $C_6H_{12}O$ (hexanedione to hexanal); (l) concentration of C_6H_6O and ratio of $C_6H_5NO_3$ to C_6H_6O
 308 (nitrophenol to phenol).

309



310 Fig. 5 summarizes the key indicators for the contrasting daytime and nighttime oxidation process. The species are
311 normalized by ΔCO , where ΔCO is the total CO concentration subtracted by the background concentration (1th percentile of
312 the dataset), to indicate the variation of species regardless of the boundary layer evolution (Gouw and Jimenez, 2009). The
313 odd oxygen O_x (O_3+NO_2) has been widely used to generally indicate the activity of daytime photochemistry (Hu et al.,
314 2017), and the enhanced moisture is main driving factor for nighttime chemistry. The O_x concentration and RH are therefore
315 used as references with which the variations of species were correlated in the day and night, respectively. As Fig. 5a shown,
316 the traffic primary emissions in both gas (traffic VOCs) and aerosol phase (HOA) declined with increased O_x by 60 % and
317 40% respectively, suggesting their roles as precursors in the daytime reaction. The produced species are oxygenated
318 SecVOC2 and OOA2, showing enhancement with O_x , peaking at midday-afternoon. This process was rapid as the SOA
319 production by a factor of 2.5 and the oxygenated VOCs production by a factor of 1.7 within 6 hours. The traffic VOCs are
320 widely observed to contribute to SOA production, with aromatic compounds serving as key precursors (Fang et al., 2021).
321 The semi-volatile nature of HOA means it could be evaporated to gas phase and further oxidized to recondense as SOA
322 (Robinson et al., 2007). The decrease rate of HOA with increased photochemical age was also found in urban environment
323 (Zhu et al., 2021), generally consistent with the reacted rate in this study. Here we linked the declining rate as a function of
324 photochemical activities for both reacted aerosol and gas phases for traffic sources. The gases evaporated from aerosol phase
325 (especially under higher temperature) and primary VOCs may be simultaneously involved in the photooxidation, further
326 contributing to the SOA formation.

327 For nocturnal oxidation shown in Fig. 5b, the reacted species are cooking VOCs and COA (decrease by 35 % and 77 %,
328 respectively), producing SecVOC1 and large-MW oxygenated VOCs, with an increase of night SOA formation by a factor
329 of 1.7. The nocturnal processes may have largely involved aqueous reactions, because the variations of reacted or produced
330 species were highly correlated with RH (Fig. 5b). The large-MW VOCs (mostly IVOCs) increased by 50% and reached
331 maxima when highest RH. This suggests the moisture may have been involved in converting some primary VOCs to IVOCs,
332 which further contribute to the SOA production during nighttime. Previous studies also found the oxidation of IVOCs from
333 cooking sources can be an important source of SOA (Zhang et al., 2020b). The evidence is given here that organic aerosols
334 and gases from cooking emission had been reacted and contributed to SOA. The production rate of $0.2 \mu\text{g m}^{-3} \text{h}^{-1}$ was
335 generally consistent with previous laboratory work using gas precursors from cooking sources ($0.07\text{-}0.5 \mu\text{g m}^{-3} \text{h}^{-1}$) (Liu et
336 al., 2017). Notably, daytime SOA had a higher oxidation state, implying the importance of photooxidation in producing
337 highly oxidized OA. This may be because of the high temperature at daytime and a species may require a lower volatility
338 (hereby more oxygenated) to be in condensed phase than at night.



339
340 Figure 5. Daytime and nighttime evolution of key species against O_x and RH respectively. (a) Daytime oxidation showing the
341 primary emissions of traffic source in gas and aerosol phases including HOA, traffic VOCs; and secondary products including
342 SecVOC2 and OOA2, with concentrations all normalized by ΔCO . (b) Nighttime oxidation showing the primary emissions of
343 cooking source in gas and aerosol phases including COA and cooking VOCs; and secondary products including SecVOC1, large-
344 MW VOC and OOA1, with concentrations all normalized by ΔCO .

345 4 Conclusion

346 In this study, organic gases and aerosols were concurrently characterized through online mass spectrometers at a
347 megacity in central China. Through the factorization analysis on the organic mass spectra, two principal sources - the traffic
348 and cooking sources were identified for both aerosol and gas phases, hereby the reacted and produced species between
349 phases were interlinked. We observed clear evidence of daytime and nighttime oxidation of source-attributed OA and VOCs.
350 Daytime photooxidation caused 60 % decrease of primary aerosol and 40 % of primary VOCs reduction for traffic sources,
351 producing oxygenated SecVOCs by a factor of 1.7 and OOA by a factor of 2.5, in a 6 hours photochemical ageing.
352 Nocturnal ageing caused a reduction of primary OA (by 77%) and primary VOCs (by 35%) from cooking sources, producing
353 oxygenated VOCs and OOA by a factor of 1.4 and 1.7, respectively. In particular, larger molecular IVOCs produced (by a
354 factor of 1.7) at night may importantly contribute to the OOA. This implies primary species in aerosol and gas phases both
355 contribute to the production of OOA. A higher oxidation state of OOA from daytime photooxidation was found than
356 nighttime, suggesting different compositions of produced OOA modulated by solar radiation and moisture, respectively. As
357 vehicle and cooking emissions are the major contributors of organic aerosols in urban areas, especially in megacities. These
358 results provide direct observations about the reaction rate for primary precursors and production rate for secondary aerosols,
359 as influenced by primary sources and meteorological conditions. The environmental policy making should therefore consider
360 the respective primary sources and ageing mechanisms for local and regional atmospheric environmental problems.

361 Data availability

362 The data in this study are available from the corresponding author upon request.



363 Author contribution

364 DL, SK, and SL led and designed the study. SL, YW, HZ, YC, SZ and DH set up and conducted the experiment. SL,
365 DL, YW, KH, XJ and SD contributed to the data analysis. QL, DZ, JS provided technical support and assistance. SL wrote
366 the manuscript draft. DL and SK provided critical review and substantially revised the manuscript. All authors read and
367 approved the final manuscript.

368 Competing interests

369 The authors declare no competing interests.

370 Acknowledgments

371 This work was supported by the National Key R&D programme of China (2019YFC0214703), National Natural
372 Science Foundation of China (Grant Nos. 42175116, 41875167).

373

374 References

- 375 Adler, G., Flores, J. M., Abo Riziq, A., Borrmann, S., and Rudich, Y.: Chemical, physical, and optical evolution of biomass burning
376 aerosols: a case study, *Atmos. Chem. Phys.*, 11, 1491–1503, <https://doi.org/10.5194/acp-11-1491-2011>, 2011.
- 377 Aiken, A., Salcedo, D., Cubison, M., Huffman, J., DeCarlo, P., Ulbrich, I., Docherty, K., Sueper, D., Kimmel, J., Worsnop, D., A, T., M,
378 N., Stone, E., Schauer, J., Volkamer, R., Fortner, E., de Foy, B., Wang, J., Laskin, A., and Jimenez, J.: Mexico City Aerosol Analysis
379 During Milagro Using High Resolution Aerosol Mass Spectrometry at the Urban Supersite (T0) - Part 1: Fine Particle Composition
380 and Organic Source Apportionment, *Atmos. Chem. Phys.*, 9, 6633–6653, <https://doi.org/10.5194/acp-9-6633-2009>, 2009.
- 381 Allan, J. D., Williams, P. I., Morgan, W. T., Martin, C. L., and Coe, H.: Contributions from transport, solid fuel burning and cooking to
382 primary organic aerosols in two UK cities, *Atmos. Chem. Phys.*, 10, 647–668, <https://doi.org/10.5194/acp-10-647-2010>, 2010.
- 383 Allan, J. D., Williams, P., Morgan, W., Martin, C., Flynn, M., Lee, J., Nemitz, E., Phillips, G., Gallagher, M., and Coe, H.: Contributions
384 from transport, solid fuel burning and cooking to primary organic aerosols in two UK cities, *Atmos. Chem. Phys.*, 10, 647–
385 668, <https://doi.org/10.5194/acp-10-647-2010>, 2010.
- 386 Bruns, E. A., El Haddad, I., Slowik, J. G., Kilic, D., Klein, F., Baltensperger, U., and Prévôt, A. S. H.: Identification of significant
387 precursor gases of secondary organic aerosols from residential wood combustion, *Sci. Rep.*, 6, 27881, <https://doi.org/10.1038/srep27881>, 2016.
- 389 Canagaratna, M. R., Jimenez, J. L., Kroll, J. H., Chen, Q., and Worsnop, D. R.: Elemental ratio measurements of organic compounds using
390 aerosol mass spectrometry: characterization, improved calibration, and implications, *Atmos. Chem. Phys.*, 15, 253–
391 272, <https://doi.org/10.5194/acp-15-253-2015>, 2015.
- 392 Canagaratna, M. R., Jayne, J. T., Jimenez, J. L., Allan, J. D., Alfarra, M. R., Zhang, Q., Onasch, T. B., Drewnick, F., Coe, H.,
393 Middlebrook, A., Delia, A., Williams, L. R., Trimborn, A. M., Northway, M. J., DeCarlo, P. F., Kolb, C. E., Davidovits, P., and
394 Worsnop, D. R.: Chemical and microphysical characterization of ambient aerosols with the aerodyne aerosol mass spectrometer,
395 *Mass. Spectrom. Rev.*, 26, 185–222, <https://doi.org/10.1002/mas.20115>, 2007.
- 396 Cappellin, L., Karl, T., Probst, M., Ismailova, O., Winkler, P. M., Soukoulis, C., Aprea, E., Mark, T. D., Gasperi, F., and Biasioli, F.: On
397 quantitative determination of volatile organic compound concentrations using proton transfer reaction time-of-flight mass
398 spectrometry, *Environ. Sci. Technol.*, 46, 2283–2290, <https://doi.org/10.1021/es203985t>, 2012.
- 399 Chen, T., Liu, J., Ma, Q., Chu, B., Zhang, P., Ma, J., Liu, Y., Zhong, C., Liu, P., Wang, Y., Mu, Y., and He, H.: Measurement report:
400 Effects of photochemical aging on the formation and evolution of summertime secondary aerosol in Beijing, *Atmos. Chem. Phys.*, 21,
401 1341–1356, <https://doi.org/10.5194/acp-21-1341-2021>, 2021.
- 402 Cheng, X., Li, H., Zhang, Y., Li, Y., Zhang, W., Wang, X., Bi, F., Zhang, H., Gao, J., Chai, F., Lun, X., Chen, Y., Gao, J., and Lv, J.:
403 Atmospheric isoprene and monoterpenes in a typical urban area of Beijing: Pollution characterization, chemical reactivity and source
404 identification, *J. Environ. Sci (China)*, 71, 150–167, <https://doi.org/10.1016/j.jes.2017.12.017>, 2018.



- 405 Claeys, M., Graham, B., Vas, G., Wu, W., Vermeylen, R., Pashynska, V., Cafmeyer, J., Cuyon, P., Andreae, M. O., and Artaxo, P.:
406 Formation of Secondary Organic Aerosols Through Photooxidation of Isoprene, *Science*, 303, 1173–1176,
407 <https://doi.org/10.1126/science.1092805>, 2004.
- 408 Decarlo, P. F., Kimmel, J. R., Trimborn, A., Northway, M. J., Jayne, J. T., Aiken, A. C., Gonin, M., Fuhrer, K., Horvath, T., and Docherty,
409 K. S.: Field-deployable, high-resolution, time-of-flight aerosol mass spectrometer, *Anal. Chem.*, 78, 8281–8289,
410 <https://doi.org/10.1021/ac061249n>, 2006.
- 411 Decarlo, P. F., Ulbrich, I. M., Crounse, J., Foy, B. D., Dunlea, E. J., Aiken, A. C., Knapp, D., Weinheimer, A. J., Campos, T., and
412 Wennberg, P. O.: Investigation of the sources and processing of organic aerosol over the Central Mexican Plateau from aircraft
413 measurements during MILAGRO, *Atmos. Chem. Phys.*, 10, 5257–5280, <https://doi.org/10.5194/acp-10-5257-2010>, 2010.
- 414 Donahue, N. M., Robinson, A. L., Stanier, C. O., and Pandis, S. N.: Coupled Partitioning, Dilution, and Chemical Aging of Semivolatile
415 Organics, *Environ. Sci. Technol.*, 2006, 40, 8, 2635–2643, <https://doi.org/10.1021/es052297c>, 2006.
- 416 Draxler, R. and Hess, G.: Description of the HYSPLIT_4 modelling system, NOAA Tech. Mem. ERL ARL-224, 1997.
- 417 Fang, H., Huang, X., Zhang, Y., Pei, C., Huang, Z., Wang, Y., Chen, Y., Yan, J., Zeng, J., Xiao, S., Luo, S., Li, S., Wang, J., Zhu, M., Fu,
418 X., Wu, Z., Zhang, R., Song, W., Zhang, G., Hu, W., Tang, M., Ding, X., Bi, X., and Wang, X.: Measurement report: Emissions of
419 intermediate-volatility organic compounds from vehicles under real-world driving conditions in an urban tunnel, *Atmos. Chem.*
420 *Phys.*, 21, 10005–10013, <https://doi.org/10.5194/acp-21-10005-2021>, 2021.
- 421 Gkatzelis, G. I., Coggon, M. M., McDonald, B. C., Peischl, J., Gilman, J. B., Aikin, K. C., Robinson, M. A., Canonaco, F., Prevot, A. S.
422 H., Trainer, M., and Warneke, C.: Observations Confirm that Volatile Chemical Products Are a Major Source of Petrochemical
423 Emissions in U.S. Cities, *Environ. Sci. Technol.*, 55, 4332–4343, <https://doi.org/10.1021/acs.est.0c05471>, 2021.
- 424 Goldstein, A. H. and Galbally, I. E.: Known and Unexplored Organic Constituents in the Earth's Atmosphere, *Environ. Sci. Technol.*, 41,
425 1514–1521, <https://doi.org/10.1021/es072476p>, 2007.
- 426 Gouw, J. D. and Jimenez, J. L.: Organic Aerosols in the Earth's Atmosphere, *Environ. Sci. Technol.*, 43, 7614–7618,
427 <https://doi.org/10.1021/es9006004>, 2009.
- 428 Gu, C., Wang, S., Zhu, J., Wu, S., Duan, Y., Gao, S., and Zhou, B.: Investigation on the urban ambient isoprene and its oxidation
429 processes, *Atmospheric Environ.*, 270, 118870, <https://doi.org/10.1016/j.atmosenv.2021.118870>, 2021.
- 430 Guo, J., Zhou, S., Cai, M., Zhao, J., Song, W., Zhao, W., Hu, W., Sun, Y., He, Y., Yang, C., Xu, X., Zhang, Z., Cheng, P., Fan, Q., Hang,
431 J., Fan, S., Wang, X., and Wang, X.: Characterization of submicron particles by time-of-flight aerosol chemical speciation monitor
432 (ToF-ACSM) during wintertime: aerosol composition, sources, and chemical processes in Guangzhou, China, *Atmos. Chem. Phys.*,
433 20, 7595–7615, <https://doi.org/10.5194/acp-20-7595-2020>, 2020.
- 434 Hallquist, M., Wenger, J. C., Baltensperger, U., Rudich, Y., Simpson, D., Claeys, M., Dommen, J., Donahue, N. M., George, C.,
435 Goldstein, A. H., Hamilton, J. F., Herrmann, H., Hoffmann, T., Iinuma, Y., Jang, M., Jenkin, M. E., Jimenez, J. L., Kiendler-Scharr,
436 A., Maenhaut, W., Mcfiggans, G., Mentel, T. F., Monod, A., Prevot, A. S. H., Seinfeld, J. H., Surratt, J. D., Szmigielski, R., and
437 Wildt, J.: The formation, properties and impact of secondary organic aerosol: current and emerging issues, *Atmos. Chem. Phys.*, 9,
438 5155–5236, <https://doi.org/10.5194/acp-9-5155-2009>, 2009.
- 439 Hartikainen, A., Yli-Pirilä, P., Tiitta, P., Leskinen, A., Kortelainen, M., Orasche, J., Schnelle-Kreis, J., Lehtinen, K., Zimmermann, R.,
440 Jokiniemi, J., and Sippula, O.: Volatile Organic Compounds from Logwood Combustion: Emissions and Transformation under Dark
441 and Photochemical Aging Conditions in a Smog Chamber, *Environ. Sci. Technol.*, 52, 4979–4988,
442 <https://doi.org/10.1021/acs.est.7b06269>, 2018.
- 443 Hatch, L. E., Yokelson, R. J., Stockwell, C. E., Veres, P. R., Simpson, I. J., Blake, D. R., Orlando, J. J., and Barsanti, K. C.: Multi-
444 instrument comparison and compilation of non-methane organic gas emissions from biomass burning and implications for smoke-
445 derived secondary organic aerosol precursors, *Atmos. Chem. Phys.*, 17, 1471–1489, <https://doi.org/10.5194/acp-17-1471-2017>, 2017.
- 446 Hayes, P. L., Ortega, A. M., Cubison, M. J., Froyd, K. D., Zhao, Y., Cliff, S. S., Hu, W. W., Toohey, D. W., Flynn, J. H., Lefter, B. L.,
447 Grossberg, N., Alvarez, S., Rappenglück, B., Taylor, J. W., Allan, J. D., Holloway, J. S., Gilman, J. B., Kuster, W. C., de Gouw, J.
448 A., Massoli, P., Zhang, X., Liu, J., Weber, R. J., Corrigan, A. L., Russell, L. M., Isaacman, G., Worton, D. R., Kreisberg, N. M.,
449 Goldstein, A. H., Thalman, R., Waxman, E. M., Volkamer, R., Lin, Y. H., Surratt, J. D., Kleindienst, T. E., Offenberg, J. H.,
450 Dusanter, S., Griffith, S., Stevens, P. S., Brioude, J., Angevine, W. M., and Jimenez, J. L.: Organic aerosol composition and sources
451 in Pasadena, California, during the 2010 CalNex campaign, *J. Geophys. Res.-Atoms.*, 118, 9233–9257,
452 <https://doi.org/10.1002/jgrd.50530>, 2013.
- 453 Heald, C. L., Jacob, D. J., Park, R. J., Russell, L. M., Huebert, B. J., Seinfeld, J. H., Liao, H., and Weber, R. J.: A large organic aerosol
454 source in the free troposphere missing from current models, *Geophys. Res. Lett.*, 32, <https://doi.org/10.1029/2005gl023831>, 2005.
- 455 Hu, D., Liu, D., Kong, S., Zhao, D., Wu, Y., Li, S., Ding, S., Zheng, S., Cheng, Y., Hu, K., Deng, Z., Wu, Y., Tian, P., Liu, Q., Huang, M.,
456 and Ding, D.: Direct Quantification of Droplet Activation of Ambient Black Carbon Under Water Supersaturation, *J. Geophys. Res.-*
457 *Atoms.*, 126, <https://doi.org/10.1029/2021jd034649>, 2021.
- 458 Hu, W., Hu, M., Hu, W.-W., Zheng, J., Chen, C., Wu, Y., and Guo, S.: Seasonal variations in high time-resolved chemical compositions,
459 sources, and evolution of atmospheric submicron aerosols in the megacity Beijing, *Atmos. Chem. Phys.*, 17, 9979–10000,
460 <https://doi.org/10.5194/acp-17-9979-2017>, 2017.



- 461 Hu, W., Hu, M., Hu, W., Jimenez, J., Yuan, B., Chen, W., Wang, M., Wu, Y., Chen, C., Wang, Z., Peng, J., Zeng, L., and Shao, M.:
462 Chemical composition, sources, and aging process of submicron aerosols in Beijing: Contrast between summer and winter, *J.*
463 *Geophys. Res.-Atoms.*, <https://doi.org/10.1002/2015JD024020>, 2016.
- 464 Hu, W. W., Hu, M., Yuan, B., Jimenez, J. L., Tang, Q., Peng, J. F., Hu, W., Shao, M., Wang, M., Zeng, L. M., Wu, Y. S., Gong, Z. H.,
465 Huang, X. F., and He, L. Y.: Insights on organic aerosol aging and the influence of coal combustion at a regional receptor site of
466 central eastern China, *Atmos. Chem. Phys.*, 13, 10095–10112, <https://doi.org/10.5194/acp-13-10095-2013>, 2013.
- 467 Huang, L., Wang, Q., Wang, Y., Emery, C., Zhu, A., Zhu, Y., Yin, S., Yarwood, G., Zhang, K., and Li, L.: Simulation of secondary
468 organic aerosol over the Yangtze River Delta region: The impacts from the emissions of intermediate volatility organic compounds
469 and the SOA modeling framework, *Atmospheric Environ.*, 246, 118079, <https://doi.org/10.1016/j.atmosenv.2020.118079>, 2021.
- 470 Huang, R. J., Zhang, Y., Bozzetti, C., Ho, K. F., Cao, J. J., Han, Y., Daellenbach, K. R., Slowik, J. G., Platt, S. M., Canonaco, F., Zotter,
471 P., Wolf, R., Pieber, S. M., Bruns, E. A., Crippa, M., Ciarelli, G., Piazzalunga, A., Schwikowski, M., Abbaszade, G., Schnelle-Kreis,
472 J., Zimmermann, R., An, Z., Szidat, S., Baltensperger, U., El Haddad, I., and Prevot, A. S.: High secondary aerosol contribution to
473 particulate pollution during haze events in China, *Nature*, 514, 218–222, <https://doi.org/10.1038/nature13774>, 2014.
- 474 Huang, X. F., He, L. Y., Hu, M., Canagaratna, M. R., Sun, Y., Zhang, Q., Zhu, T., Xue, L., Zeng, L. W., Liu, X. G., Zhang, Y. H., Jayne,
475 J. T., Ng, N. L., and Worsnop, D. R.: Highly time-resolved chemical characterization of atmospheric submicron particles during 2008
476 Beijing Olympic Games using an Aerodyne High-Resolution Aerosol Mass Spectrometer, *Atmos. Chem. Phys.*, 10, 8933–8945,
477 <https://doi.org/10.5194/acp-10-8933-2010>, 2010.
- 478 Jayne, J. T., Leard, D. C., Zhang, X., Davidovits, P., Smith, K. A., Kolb, C. E., and Worsnop, D. R.: Development of an Aerosol Mass
479 Spectrometer for Size and Composition Analysis of Submicron Particles, *Aerosol. Sci. Technol.*, 33, 49–70,
480 [https://doi.org/10.1016/S0021-8502\(98\)00158-X](https://doi.org/10.1016/S0021-8502(98)00158-X), 2000.
- 481 Jokinen, T., Berndt, T., Makkonen, R., Kerminen, V. M., and Sipil, M.: Production of extremely low volatile organic compounds from
482 biogenic emissions: Measured yields and atmospheric implications, *Proc. Natl. Acad. Sci.*, 112, 7123–7128,
483 <https://doi.org/10.1073/pnas.1423977112>, 2015.
- 484 Jordan, C., Fitz, E., Hagan, T., Sive, B., Frinak, E., Haase, K., Cottrell, L., Buckley, S., and Talbot, R.: Long-term study of VOCs
485 measured with PTR-MS at a rural site in New Hampshire with urban influences, *Atmos. Chem. Phys.*, 9, 4677–
486 4697, <https://doi.org/10.5194/acp-9-4677-2009>, 2009.
- 487 Klein, F., Platt, S. M., Farren, N. J., Detournay, A., Bruns, E. A., Bozzetti, C., Daellenbach, K. R., Kilic, D., Kumar, N. K., Pieber, S. M.,
488 Slowik, J. G., Temime-Roussel, B., Marchand, N., Hamilton, J. F., Baltensperger, U., Prevot, A. S., and El Haddad, I.:
489 Characterization of Gas-Phase Organics Using Proton Transfer Reaction Time-of-Flight Mass Spectrometry: Cooking Emissions,
490 *Environ. Sci. Technol.*, 50, 1243–1250, <https://doi.org/10.1021/acs.est.5b04618>, 2016.
- 491 Knote, C., Hodzic, A., Jimenez, J. L., Volkamer, R., Orlando, J. J., Baidar, S., Brioude, J., Fast, J. D., Gentner, D. R., Goldstein, A. H.,
492 Hayes, P. L., Knighton, W., Oetjen, H., Setyan, A., Stark, H., Thalman, R. M., Tyndall, G. S., Washenfelder, R. A., Waxman, E., and
493 Zhang, Q.: Simulation of semi-explicit mechanisms of SOA formation from glyoxal in aerosol in a 3D model, *Atmos. Chem. Phys.*,
494 14, 6213–6239, <https://doi.org/10.5194/acp-14-6213-2014>, 2014.
- 495 Kroll, J. and Seinfeld, J.: Chemistry of secondary organic aerosol: Formation and evolution of low-volatility organics in the atmosphere,
496 *Atmospheric Environ.*, 42, 3593–3624, <https://doi.org/10.1016/j.atmosenv.2008.01.003>, 2008.
- 497 Laborde, M., Schnaiter, M., Linke, C., Saathoff, H., Naumann, K.-H., Möhler, O., Berlenz, S., Wagner, U., Taylor, J., Liu, D., Flynn, M.,
498 Allan, J., Coe, H., Heimerl, K., Dahlkötter, F., Weinzierl, B., Wollny, A. G., Zanatta, M., Cozic, J., and Gysel, M.: Single Particle
499 Soot Photometer intercomparison at the AIDA chamber, *Atmos. Meas. Tech.*, 5, 3077–3097, [https://doi.org/10.5194/amt-5-3077-](https://doi.org/10.5194/amt-5-3077-2012)
500 2012, 2012.
- 501 Lanz, V. A., Alfarra, M. R., Baltensperger, U., Buchmann, B., Hueglin, C., Szidat, S., Wehrli, M. N., Wacker, L., Weimer, S., and Caseiro,
502 A.: Source attribution of submicron organic aerosols during wintertime inversions by advanced factor analysis of aerosol mass
503 spectra, *Environ. Sci. Technol.* 2008, 42, 1, 214–220, <https://doi.org/10.1021/es0707207>, 2008.
- 504 Li, J., Cao, L., Gao, W., He, L., Yan, Y., He, Y., Pan, Y., Ji, D., Liu, Z., and Wang, Y.: Seasonal variations in the highly time-resolved
505 aerosol composition, sources and chemical processes of background submicron particles in the North China Plain, *Atmos. Chem.*
506 *Phys.*, 21, 4521–4539, <https://doi.org/10.5194/acp-21-4521-2021>, 2021a.
- 507 Li, S., Liu, D., Hu, D., Kong, S., Wu, Y., Ding, S., Cheng, Y., Qiu, H., Zheng, S., Yan, Q., Zheng, H., Hu, K., Zhang, J., Zhao, D., Liu, Q.,
508 Sheng, J., Ye, J., He, H., and Ding, D.: Evolution of Organic Aerosol From Wood Smoke Influenced by Burning Phase and Solar
509 Radiation, *J. Geophys. Res.-Atoms.*, 126, <https://doi.org/10.1029/2021JD034534>, 2021b.
- 510 Li, Y., Pöschl, U., and Shiraiwa, M.: Molecular corridors and parameterizations of volatility in the chemical evolution of organic aerosols,
511 *Atmos. Chem. Phys.*, 16, 3327–3344, <https://doi.org/10.5194/acp-16-3327-2016>, 2016.
- 512 Lin, G., Penner, J. E., Sillman, S., Taraborrelli, D., and Lelieveld, J.: Global modeling of SOA formation from dicarbonyls, epoxides,
513 organic nitrates and peroxides, *Atmos. Chem. Phys.*, 12, 4743–4774, <https://doi.org/10.5194/acp-12-4743-2012>, 2012.
- 514 Lin, Y. H., Zhang, H., Pye, H. O., Zhang, Z., Marth, W. J., Park, S., Arashiro, M., Cui, T., Budisulistiorini, S. H., Sexton, K. G., Vizuete,
515 W., Xie, Y., Luecken, D. J., Piletic, I. R., Edney, E. O., Bartolotti, L. J., Gold, A., and Surratt, J. D.: Epoxide as a precursor to



- 516 secondary organic aerosol formation from isoprene photooxidation in the presence of nitrogen oxides, *Proc. Natl. Acad. Sci.*, 110,
517 6718–6723, <https://doi.org/10.1073/pnas.1221150110>, 2013.
- 518 Liu, D., Flynn, M., Gysel, M., Targino, A., Crawford, I., Bower, K., Choularton, T., Jurányi, Z., Steinbacher, M., Hüglin, C., Curtius, J.,
519 Kampus, M., Petzold, A., Weingartner, E., and Baltensperger, U.: Single particle characterization of black carbon aerosols at a
520 tropospheric alpine site in Switzerland, *Atmos. Chem. Phys.*, 10, 7389–7407, <https://doi.org/10.5194/acpd-10-8765-2010>, 2010.
- 521 Liu, T., Wang, Z., Huang, D. D., Wang, X., and Chan, C. K.: Significant Production of Secondary Organic Aerosol from Emissions of
522 Heated Cooking Oils, *Environ. Sci. Technol. Lett.*, 5, 32–37, <https://doi.org/10.1021/acs.estlett.7b00530>, 2017.
- 523 Middlebrook, A. M., Bahreini, R., Jimenez, J. L., and Canagaratna, M. R.: Evaluation of Composition-Dependent Collection Efficiencies
524 for the Aerodyne Aerosol Mass Spectrometer using Field Data, *Aerosol. Sci. Technol.*, 46, 258–271,
525 <https://doi.org/10.1080/02786826.2011.620041>, 2012.
- 526 Mohr, C., DeCarlo, P. F., Heringa, M. F., Chirico, R., Slowik, J. G., Richter, R., Reche, C., Alastuey, A., Querol, X., Seco, R., Peñuelas,
527 J., Jiménez, J. L., Crippa, M., Zimmermann, R., Baltensperger, U., and Prévôt, A. S. H.: Identification and quantification of organic
528 aerosol from cooking and other sources in Barcelona using aerosol mass spectrometer data, *Atmos. Chem. Phys.*, 12, 1649–1665,
529 <https://doi.org/10.5194/acp-12-1649-2012>, 2012.
- 530 Moody, J. L. and Galloway, J. N.: Quantifying the relationship between atmospheric transport and the chemical composition of
531 precipitation on Bermuda, *Tellus*, 40B, 463–479, <https://doi.org/10.1111/j.1600-0889.1988.tb00117.x>, 1988.
- 532 Morgan, W., Allan, J., Bower, K., Highwood, E., Liu, D., McMeeking, G., Northway, M., Williams, P., Krejci, R., and H, C.: Airborne
533 measurements of the spatial distribution of aerosol chemical composition across Europe and evolution of the organic fraction, *Atmos.*
534 *Chem. Phys.*, 10, 4065–4083, <https://doi.org/10.5194/acp-10-4065-2010>, 2010.
- 535 N. L., N. G., Canagaratna, M. R., Jimenez, I. L., Zhang, Q., Ulbrich, I. M., and Worsnop, D. R.: Real-time methods for estimating organic
536 component mass concentrations from aerosol mass spectrometer data, *Environ. Sci. Technol.*, 45, 910–916,
537 <https://doi.org/10.1021/es102951k>, 2011.
- 538 Ng, N., Jimenez, J., Chhabra, P., Seinfeld, J., and Worsnop, D.: Changes in organic aerosol composition with aging inferred from aerosol
539 mass spectra, *Atmos. Chem. Phys.*, 11, 6465–6474, <https://doi.org/10.5194/acp-11-6465-2011>, 2011
- 540 Ortiz-Montalvo, D. L., Hakkinen, S. A., Schwier, A. N., Lim, Y. B., McNeill, V. F., and Turpin, B. J.: Ammonium addition (and aerosol
541 pH) has a dramatic impact on the volatility and yield of glyoxal secondary organic aerosol, *Environ. Sci. Technol.*, 48, 255–262,
542 <https://doi.org/10.1021/es4035667>, 2014.
- 543 Paatero, P. and Tapper, U.: Positive Matrix Factorization: A Non-Negative Factor Model with Optimal Utilization of Error Estimates of
544 Data Values, *Environmetrics*, 5, 111–126, <https://doi.org/10.1002/env.3170050203>, 1994.
- 545 Poschl, U.: Atmospheric aerosols: composition, transformation, climate and health effects, *Angew. Chem. Int. Ed. Engl.*, 44, 7520–7540,
546 <https://doi.org/10.1002/anie.200501122>, 2005.
- 547 Robinson, A. L., Donahue, N. M., Shrivastava, M. K., Weitkamp, E. A., Sage, A. M., Grieshop, A. P., Lane, T. E., Pierce, J. R., and
548 Pandis, S. N.: Rethinking organic aerosols: semivolatile emissions and photochemical aging, *Science*, 315, 1259–1262,
549 <https://doi.org/10.1126/science.1133061>, 2007.
- 550 Rogge, W. F., Hildemann, L. M., Mazurek, M. A., Cass, G. R., and Simoneit, B.: Sources of fine organic aerosol. 1. Charbroilers and meat
551 cooking operations, *Environ. Sci. Technol.*, 25, 1112–1125, <https://doi.org/10.1021/es00018a015>, 1991.
- 552 Sareen, N., Moussa, S. G., and McNeill, V. F.: Photochemical aging of light-absorbing secondary organic aerosol material, *J. Phys. Chem.*
553 *A.*, 117, 2987–2996, <https://doi.org/10.1021/jp309413j>, 2013.
- 554 Schwarz, J., Gao, R., Spackman, J. R., Watts, L., Thomson, D. S., Fahey, D., Ryerson, T., Peischl, J., Holloway, J., Trainer, M., Frost, G.,
555 Baynard, T., Lack, D., de Gouw, J., warneke, C., and Del Negro, L.: Measurement of the mixing state, mass, and optical size of
556 individual black carbon particles in urban and biomass burning emissions, *Geophys. Res. Lett.*, 35, L13810,
557 <https://doi.org/10.1029/2008GL033968>, 2008.
- 558 Seinfeld, J., Bretherton, C., Carslaw, K., Coe, H., DeMott, P., Dunlea, E., Feingold, G., Ghan, S., Guenther, A., Kahn, R., Kraucunas, I.,
559 Kreidenweis, S., Molina, M., Nenes, A., Penner, J., Prather, K., Ramanathan, V., Ramaswamy, V., Rasch, P., and Wood, R.:
560 Improving our fundamental understanding of the role of aerosol–cloud interactions in the climate system, *Proc. Natl. Acad. Sci.*, 113,
561 5781–5790, <https://doi.org/10.1073/pnas.1514043113>, 2016.
- 562 Shrivastava, M., Easter, R. C., Liu, X., Zelenyuk, A., Singh, B., Zhang, K., Ma, P.-L., Chand, D., Ghan, S., Jimenez, J. L., Zhang, Q., Fast,
563 J., Rasch, P. J., and Tiitta, P.: Global transformation and fate of SOA: Implications of low-volatility SOA and gas-phase
564 fragmentation reactions, *J. Geophys. Res.-Atoms.*, 120, 4169–4195, <https://doi.org/10.1002/2014jd022563>, 2015.
- 565 Shrivastava, M., Cappa, C. D., Fan, J., Goldstein, A. H., Guenther, A. B., Jimenez, J. L., Kuang, C., Laskin, A., Martin, S. T., Ng, N. L.,
566 Petaja, T., Pierce, J. R., Rasch, P. J., Roldin, P., Seinfeld, J. H., Shilling, J., Smith, J. N., Thornton, J. A., Volkamer, R., Wang, J.,
567 Worsnop, D. R., Zaveri, R. A., Zelenyuk, A., and Zhang, Q.: Recent advances in understanding secondary organic aerosol:
568 Implications for global climate forcing, *Rev. Geophys.*, 55, 509–559, <https://doi.org/10.1002/2016rg000540>, 2017.
- 569 Slowik, J. G., Vlasenko, A., McGuire, M., Evans, G. J., and Abbatt, J. P. D.: Simultaneous factor analysis of organic particle and gas mass
570 spectra: AMS and PTR-MS measurements at an urban site, *Atmos. Chem. Phys.*, 10, 1969–1988, <https://doi.org/10.5194/acp-10-1969-2010>, 2010.
- 571



- 572 Sun, Y., Jiang, Q., Wang, Z., Fu, P., Li, J., Yang, T., and Yin, Y.: Investigation of the sources and evolution processes of severe haze
573 pollution in Beijing in January 2013, *J. Geophys. Res.-Atoms.*, 119, 4380–4398, <https://doi.org/10.1002/2014jd021641>, 2014.
- 574 Sun, Y. L., Zhang, Q., Schwab, J. J., Demerjian, K. L., Chen, W. N., Bae, M. S., Hung, H. M., Hogrefe, O., Frank, B., Rattigan, O. V., and
575 Lin, Y. C.: Characterization of the sources and processes of organic and inorganic aerosols in New York city with a high-resolution
576 time-of-flight aerosol mass spectrometer, *Atmos. Chem. Phys.*, 11, 1581–1602, <https://doi.org/10.5194/acp-11-1581-2011>, 2011.
- 577 Ulbrich, I., Zhang, Q., Worsnop, D., and Jimenez, J.: Interpretation of organic components from Positive Matrix Factorization of aerosol
578 mass spectrometric data, *Atmos. Chem. Phys.*, 9, 2891–2918, <https://doi.org/10.5194/acp-9-2891-2009>, 2009
- 579 von Schneidmesser, E., Monks, P. S., Gros, V., Gauduin, J., and Sanchez, O.: How important is biogenic isoprene in an urban
580 environment? A study in London and Paris, *Geophys. Res. Lett.*, 38, <https://doi.org/10.1029/2011gl048647>, 2011.
- 581 Wang, J., Ye, J., Liu, D., Wu, Y., Zhao, J., Xu, W., Xie, C., Shen, F., Zhang, J., Ohno, P. E., Qin, Y., Zhao, X., Martin, S. T., Lee, A. K.
582 Y., Fu, P., Jacob, D. J., Zhang, Q., Sun, Y., Chen, M., and Ge, X.: Characterization of submicron organic particles in Beijing during
583 summertime: comparison between SP-AMS and HR-AMS, *Atmos. Chem. Phys.*, 20, 14091–14102, <https://doi.org/10.5194/acp-20-14091-2020>, 2020a.
- 584
- 585 Wang, J., Ye, J., Zhang, Q., Zhao, J., Wu, Y., Li, J., Liu, D., Li, W., Zhang, Y., Wu, C., Xie, C., Qin, Y., Lei, Y., Huang, X., Guo, J., Liu,
586 P., Fu, P., Li, Y., Lee, H. C., Choi, H., Zhang, J., Liao, H., Chen, M., Sun, Y., Ge, X., Martin, S. T., and Jacob, D. J.: Aqueous
587 production of secondary organic aerosol from fossil-fuel emissions in winter Beijing haze, *Proc. Natl. Acad. Sci.*, 118,
588 <https://doi.org/10.1073/pnas.2022179118>, 2021.
- 589 Wang, L., Slowik, J. G., Tripathi, N., Bhattu, D., and Prévôt, A.: Source characterization of volatile organic compounds measured by
590 proton-transfer-reaction time-of-flight mass spectrometers in Delhi, India, *Atmos. Chem. Phys.*, 20, 9753–
591 9770, <https://doi.org/10.5194/acp-20-9753-2020>, 2020.
- 592 Xu, J., Zhang, Q., Chen, M., Ge, X., Ren, J., and Qin, D.: Chemical composition, sources, and processes of urban aerosols during
593 summertime in northwest China: insights from high-resolution aerosol mass spectrometry, *Atmos. Chem. Phys.*, 14, 12593–12611,
594 <https://doi.org/10.5194/acp-14-12593-2014>, 2014.
- 595 Xu, W., Sun, Y., Wang, Q., Zhao, J., Wang, J., Ge, X., Xie, C., Zhou, W., Du, W., Li, J., Fu, P., Wang, Z., Worsnop, D. R., and Coe, H.:
596 Changes in Aerosol Chemistry From 2014 to 2016 in Winter in Beijing: Insights From High-Resolution Aerosol Mass Spectrometry,
597 *J. Geophys. Res.-Atoms.*, 124, 1132–1147, <https://doi.org/10.1029/2018jd029245>, 2019.
- 598 Zhang, H., Zhang, Y., Huang, Z., Acton, W. J. F., Wang, Z., Nemitz, E., Langford, B., Mullinger, N., Davison, B., Shi, Z., Liu, D., Song,
599 W., Yang, W., Zeng, J., Wu, Z., Fu, P., Zhang, Q., and Wang, X.: Vertical profiles of biogenic volatile organic compounds as
600 observed online at a tower in Beijing, *J. Environ. Sci (China)*, 95, 33–42, <https://doi.org/10.1016/j.jes.2020.03.032>, 2020a.
- 601 Zhang, Q., Jimenez, J. L., Canagaratna, M. R., Allan, J. D., Coe, H., Ulbrich, I., Alfarra, M. R., Takami, A., Middlebrook, A. M., Sun, Y.
602 L., Dzepina, K., Dunlea, E., Docherty, K., DeCarlo, P. F., Salcedo, D., Onasch, T., Jayne, J. T., Miyoshi, T., Shimojo, A.,
603 Hatakeyama, S., Takegawa, N., Kondo, Y., Schneider, J., Drewnick, F., Borrmann, S., Weimer, S., Demerjian, K., Williams, P.,
604 Bower, K., Bahreini, R., Cottrell, L., Griffin, R. J., Rautiainen, J., Sun, J. Y., Zhang, Y. M., and Worsnop, D. R.: Ubiquity and
605 dominance of oxygenated species in organic aerosols in anthropogenically-influenced Northern Hemisphere midlatitudes, *Geophys.
606 Res. Lett.*, 34, <https://doi.org/10.1029/2007gl029979>, 2007.
- 607 Zhang, Z., Zhu, W., Hu, M., Wang, H., Chen, Z., Shen, R., Yu, Y., Tan, R., and Guo, S.: Secondary Organic Aerosol from Typical
608 Chinese Domestic Cooking Emissions, *Environ. Sci. Technol. Lett.*, 8, 24–31, <https://doi.org/10.1021/acs.estlett.0c00754>, 2020b.
- 609 Zhao, Y., Nguyen, N. T., Presto, A. A., Hennigan, C. J., May, A. A., and Robinson, A. L.: Intermediate Volatility Organic Compound
610 Emissions from On-Road Diesel Vehicles: Chemical Composition, Emission Factors, and Estimated Secondary Organic Aerosol
611 Production, *Environ. Sci. Technol.*, 49, 11516–11526, <https://doi.org/10.1021/acs.est.5b02841>, 2015.
- 612 Zheng, H., Kong, S., Chen, N., Yan, Y., Liu, D., Zhu, B., Xu, K., Cao, W., Ding, Q., Lan, B., Zhang, Z., Zheng, M., Fan, Z., Cheng, Y.,
613 Zheng, S., Yao, L., Bai, Y., Zhao, T., and Qi, S.: Significant changes in the chemical compositions and sources of PM_{2.5} in Wuhan
614 since the city lockdown as COVID-19, *Sci. Total. Environ.*, 739, 140000, <https://doi.org/10.1016/j.scitotenv.2020.140000>, 2020.
- 615 Zheng, H., Kong, S., Yan, Q., Wu, F., Cheng, Y., Zheng, S., Wu, J., Yang, G., Zheng, M., Tang, L., Yin, Y., Chen, K., Zhao, T., Liu, D.,
616 Li, S., Qi, S., Zhao, D., Zhang, T., Ruan, J., and Huang, M.: The impacts of pollution control measures on PM_{2.5} reduction: Insights
617 of chemical composition, source variation and health risk, *Atmospheric. Environ.*, 197, 103–117,
618 <https://doi.org/10.1016/j.atmosenv.2018.10.023>, 2019.
- 619 Zhou, X., Li, Z., Zhang, T., Wang, F., Wang, F., Tao, Y., Zhang, X., Wang, F., and Huang, J.: Volatile organic compounds in a typical
620 petrochemical industrialized valley city of northwest China based on high-resolution PTR-MS measurements: Characterization,
621 sources and chemical effects, *Sci. Total. Environ.*, 671, 883–896, <https://doi.org/10.1016/j.scitotenv.2019.03.283>, 2019.
- 622 Zhu, W., Guo, S., Zhang, Z., Wang, H., Yu, Y., Chen, Z., Shen, R., Tan, R., Song, K., Liu, K., Tang, R., Liu, Y., Lou, S., Li, Y., Zhang,
623 W., Zhang, Z., Shuai, S., Xu, H., Li, S., Chen, Y., Hu, M., Canonaco, F., and Prévôt, A. S. H.: Mass spectral characterization of
624 secondary organic aerosol from urban cooking and vehicular sources, *Atmos. Chem. Phys.*, 21, 15065–15079,
625 <https://doi.org/10.5194/acp-21-15065-2021>, 2021.
- 626